The Astrophysical Journal, 707:705–715, 2009 December 10 doi:10.1088/0004-637X/707/1/705

SPITZER OBSERVATIONS OF THE λ ORIONIS CLUSTER. I. THE FREQUENCY OF YOUNG DEBRIS DISKS AT 5 Myr

Jesús Hernández[1], Nuria Calvet[2], L. Hartmann[2], J. Muzerolle[3], R. Gutermuth[4,5], and J. Stauffer[6]
[1] Centro de Investigaciones de Astronomía, Apdo. Postal 264, Mérida 5101-A, Venezuela; jesush@cida.ve
[2] Department of Astronomy, University of Michigan, 830 Dennison Building, 500 Church Street, Ann Arbor, MI 48109, USA
[3] Space Telescope Science Institute, 3700 San Martin Dr., Baltimore, MD 21218, USA
[4] Five Colleges Astronomy Department, Smith College, Northampton, MA 01027, USA
[5] Department of Astronomy, University of Massachusetts, Amherst, MA 01003, USA
[6] *Spitzer* Science Center, Caltech M/S 220-6, 1200 East California Boulevard, Pasadena, CA 91125, USA
Received 2009 June 8; accepted 2009 October 22; published 2009 November 25

ABSTRACT

We present IRAC/MIPS *Spitzer* observations of intermediate-mass stars in the 5 Myr old λ Orionis cluster. In a representative sample of stars earlier than F5 (29 stars), we find a population of nine stars with varying degree of moderate 24 μm excess comparable to those produced by debris disks in older stellar groups. As expected in debris disks systems, those stars do not exhibit emission lines in their optical spectra. We also include in our study the star HD 245185, a known Herbig Ae object which displays excesses in all *Spitzer* bands and shows emission lines in its spectrum. We compare the disk population in the λ Orionis cluster with the disk census in other stellar groups studied using similar methods to detect and characterize their disks and spanning a range of ages from 3 Myr to 10 Myr. We find that for stellar groups of 5 Myr or older the observed disk frequency in intermediate-mass stars (with spectral types from late B to early F) is higher than in low-mass stars (with spectral types K and M). This is in contradiction with the observed trend for primordial disk evolution, in which stars with higher stellar masses dissipate their primordial disks faster. At 3 Myr, the observed disk frequency in intermediate-mass stars is still lower than for low-mass stars indicating that second generation dusty disks start to dominate the disk population at 5 Myr for intermediate-mass stars. This result agrees with recent models of evolution of solids in the region of the disk where icy objects form (>30 AU), which suggest that at 5–10 Myr collisions start to produce large amount of dust during the transition from runaway to oligarchic growth (reaching sizes of ∼500 km) and then dust production peaks at 10–30 Myr, when objects reach their maximum size (⩾1000 km).

Key words: infrared: stars – open clusters and associations: individual (λ Orionis cluster) – planetary systems: protoplanetary disks – stars: formation – stars: pre-main sequence

Online-only material: color figures

1. INTRODUCTION

Planets are thought to form in circumstellar disks of dust and gas that result from the collapse of rotating molecular cloud cores during the star-forming process. These primordial optically thick disks evolve due to viscous processes by which the disk is accreting material onto the star while expanding to conserve angular momentum (Hartmann et al. 1998). In addition, dust grains in the disk are expected to grow in size and settle toward the mid-plane of the disk (Weidenschilling 1997), where planetesimals and planets can be formed (Backman & Paresce 1993; Kenyon & Bromley 2009). The dispersal of primordial disks operates less efficiently for stars with lower masses (Muzerolle et al. 2003; Sicilia-Aguilar et al. 2005; Lada et al. 2006; Carpenter et al. 2006; Hernández et al. 2007a; Kennedy & Kenyon 2009). Particularly, for low-mass stars (K5 or later), 90% of the stars lose their primordial disks by about 5–7 Myr (e.g., Haisch et al. 2001; Hernández et al. 2008), while for objects in the mass range of Herbig Ae/Be (HAeBe; types B, A, or F early) stars, the corresponding timescale for primordial disk dissipation is less than 3 Myr (Hernández et al. 2005).

The HAeBe stars, which have primordial optically thick disks, are the precursors of intermediate-mass stars with debris disks (like Vega or β Pic). Since the estimated lifetime for circumstellar dust grains due to radiation pressure, sublimation, and Poynting–Robertson drag is significantly smaller than the estimated ages for the stellar systems, the gas-poor disks observed in Vega-type objects must be replenished from a reservoir, such as sublimation of comets or collisions between parent bodies (Chen 2006; Kenyon & Bromley 2004; Dominik & Decin 2003). Most observational studies of the evolution of debris disks have focused on the long timescales (e.g., Decin et al. 2003; Rieke et al. 2005; Su et al. 2006; Siegler et al. 2007; Carpenter et al. 2009). These studies show that the luminosities of the debris disks decay following a simple power law (with characteristic timescales of several hundred millions years), as the debris reservoir of collisional parent bodies diminishes and the dust is removed (Kenyon & Bromley 2004; Dominik & Decin 2003). Observations suggest a peak in the debris disk phenomenon in intermediate-mass stars at 10–30 Myr (Hernández et al. 2006; Currie et al. 2008b); at the peak, debris disks are more frequent and have larger infrared excesses. These observational results are supported by theoretical models of evolution of solids in the disk (Kenyon & Bromley 2004, 2008). Since debris disks may trace active planet formation (Greenberg et al. 1978; Backman & Paresce 1993; Kenyon & Bromley 2008; Wyatt 2008; Cieza 2008), studies of debris disks younger than 10–30 Myr are crucial to understanding the processes in which primordial disks evolve to planetary systems.

The λ Orionis cluster (also known as Collinder 69) represents a unique laboratory for studies of disk evolution because it is reasonably near and relatively populous, making possible statistically significant studies of disk properties in a wide range of stellar masses. Based on main-sequence fitting of early-type

stars, Murdin & Penston (1977) obtained a distance of 400 ± 40 pc and an age of 4 Myr. Similarly, using Stromgren photometry and main-sequence fitting, Dolan & Mathieu (2001) derived a distance of 450 ± 50 pc and a turnoff age of 6 Myr. Recently, Mayne & Naylor (2008) reported that the λ Orionis cluster and the σ Orionis cluster have an age of 3 Myr. However, their disk frequencies (Barrado y Navascués et al. 2007; Hernández et al. 2007a) and comparison between empirical isochrones (Hernández et al. 2008) suggest that the λ Orionis cluster is older than the σ Orionis cluster. For consistency with previous studies of disk and stellar population, we assume a distance of 450 pc and an age of 5 Myr (see Mathieu 2008).

The unprecedented sensitivity and spatial resolution provided by the *Spitzer Space Telescope* in the near- and mid-infrared windows are powerful tools to expand significantly our understanding of star and planet formation processes. In this contribution, we analyze the near- and mid-infrared properties of intermediate-mass stars in the λ Orionis cluster. This paper is organized as follows. In Section 2, we describe the observational data and the selection of intermediate-mass star in the cluster. In Section 3, we present the method for identifying stars with infrared excesses. In Section 4, we compare the disk population of the λ Orionis cluster with results from other stellar groups inferring the nature of disk emissions around intermediate-mass stars. Finally, we give our conclusions in Section 5.

2. OBSERVATIONS

2.1. Spitzer Observations

We have obtained near-infrared and mid-infrared data of the λ Orionis cluster using the Infrared Array Camera(IRAC; Fazio et al. 2004) with its four photometric channels (3.6, 4.5, 5.8, and 8.0 μm) and the 24 μm band of the Multiband Imaging Spectrometer for *Spitzer* (MIPS; Rieke et al. 2004) on board the *Spitzer Space Telescope*. These data were collected in mapping mode during 2004 October 11 (IRAC) and March 15 (MIPS) as part of G. Fazio's Guaranteed Time Observations in *Spitzer* program 37.

The IRAC observations were done using a standard raster map with 280″ offsets, to provide maximum areal coverage while still allowing ∼20″ overlap between frames in order to facilitate accurate mosaicking of the data. Images were obtained in high dynamic range (HDR) mode, in which a short integration (1 s) is immediately followed by a long integration (26.8 s). Standard Basic Calibrated Data (BCD) products from version S14.0.0 of the Spitzer Science Center's IRAC pipeline were used to make the final mosaics. Post-BCD data treatment was performed using custom IDL software (Gutermuth et al. 2004) that includes modules for detection and correction of bright source artifacts, detection, and removal of cosmic-ray hits, construction of the long and short exposure HDR mosaics, and the merger of those mosaics to yield the final science images with a scale of 1.″22 pixel^{-1}. Since mosaics of channels 4.5 and 8.0 μm have a 6.′5 displacement to the north from the mosaics of channels 3.6 and 5.8 μm, the region with the complete IRAC data set (57.′6 × 54.′6; hereafter IRAC region) is smaller than the field of view (FOV) of individual mosaics (57.′6 × 61.′2). IRAC point-source photometry was obtained using the *apphot* package in IRAF, with an aperture radius of 3.″7 and a background annulus from 3.″7 to 8.″6. We adopted zero-point magnitudes for the standard aperture radius (12″) and background annulus (12″–22.″4) of 19.665, 18.928, 16.847, and 17.391 in the [3.6], [4.5], [5.8], and [8.0] bands, respectively. Aperture corrections were made using the values described in IRAC Data Handbook (Reach et al. 2006). Final photometric errors include the uncertainties in the zero-point magnitudes (∼0.02 mag).

MIPS observations were made using medium scan mode with full-array cross-scan overlap, resulting in a total effective exposure time per pointing of 40 s. MIPS observations cover more than 99% of the IRAC region. The images were processed using the MIPS instrument team Data Analysis Tool (DAT), which calibrates the data and applies a distortion correction to each individual exposure before combining it into a final mosaic (Gordon et al. 2005). A second flat correction was also done to each image using a median of all the images in order to correct for dark latents and scattered light background gradients. The second flat correction is determined by creating a median image of all the data in a given scan leg, and then dividing each individual image in that scan leg by that median. Bright sources and extended regions are masked out of the data before creation of the median, so the nebulosity seen in the map has a negligible effect on any noise that might be added by the second flat. We obtained point-source photometry at 24 μm with IRAF/*daophot* point-spread function fitting, using an aperture size of about 5.″7 and an aperture correction factor of 1.73 derived from the STinyTim PSF model. The aperture size corresponds to the location of the first airy dark ring, and was chosen to minimize effects of source crowding and background inhomogeneities. The absolute flux calibration uncertainty is ∼4% (Engelbracht et al. 2007). The photometric uncertainties are dominated by the background/photon noise. Our final 24 μm flux measurements are complete down to about 0.8 mJy.

2.2. Sample Selection and Optical Spectra

Our procedure for identifying the disk population around intermediate-mass stars in the λ Orionis cluster is similar to that described in Hernández et al. (2006). To find the bright stellar population of the λ Orionis cluster, we selected from the Two Micron All Sky Survey (2MASS) catalog[7] stars with $J \leqslant 11$. This limit was calculated using the V magnitude (Cox 2000) and the $V-J$ color (Kenyon & Hartmann 1995) for a main-sequence star with spectral type F5 located at 450 pc (Dolan & Mathieu 2001; Mathieu 2008) and assuming a visual extinction of $A_V \sim 0.4$ (Diplas & Savage 1994). The reddening in the 2MASS bands was calculated from the assumed visual extinction using the Cardelli et al. (1989) extinction law with $R_V = 3.1$. Our preliminary sample includes 159 stars located in the IRAC region.

We found two relatively bright stars ($V < 12$) without 2MASS counterpart when comparing our preliminary sample with photometric studies of the bright population in the λ Orionis cluster (Dolan & Mathieu 2001; Murdin & Penston 1977; Duerr et al. 1982). One star (HD36862) is a close companion (⩽3″) of the central bright star of the cluster (the λ Orionis star), not resolved in the IRAC/MIPS images. The other star, HD245168, was included previously as member of the λ Orionis cluster with spectral type B9 (Dolan & Mathieu 2001; Murdin & Penston 1977). Visual inspection of the 2MASS images reveals that HD 245168 is a stellar source not included in the 2MASS catalog. We estimated 2MASS photometry for this source using differential photometry. We use 2MASS sources located inside 6′ of radius to get the median value of differential photometry between the 2MASS magnitudes and the instrumental magnitudes obtained on the 2MASS images using

[7] Vizier Online Data Catalog, 2246 (Cutri et al. 2003).

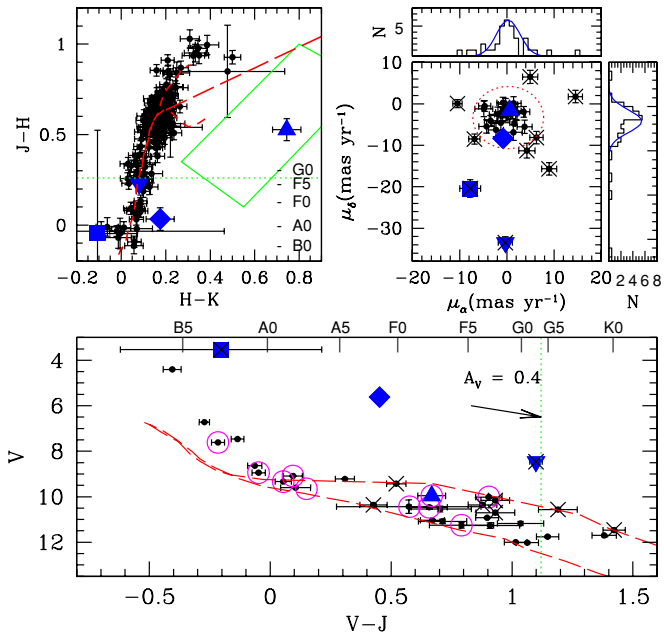

Figure 1. Diagrams illustrating the selection of photometric candidates of the λ Orionis cluster. The HAeBe star HD 245185 (triangle), the star λ Orionis (square), the stars HD 36881 (diamond), and HD 37148 (inverse triangle) are marked. The upper left panel shows the 2MASS color–color diagram. The standard sequences from Bessell & Brett (1988) are shown in dashed lines. The locus of the CTTS (Meyer et al. 1997) and the HAeBe stars (Hernández et al. 2005) are defined by a long-dashed line and by a solid box, respectively. The photometric limit for a F5 star with reddening of $A_V = 0.4$ is represented by a dotted line in the upper left panel and in the bottom panel. We selected stars below the photometric limit. The upper right panel shows the vector point diagram for stars selected in the upper left panel. In general, these stars have similar proper motions; however, since the SNe explosion could affect the kinematic properties of the cluster, kinematic criteria cannot be used alone to reject probable member of the cluster. Stars with discrepant proper motion are plotted with crosses. Finally, the bottom panel shows the color–magnitude diagram $V-J$ vs. V. Our sample of early-type star in the λ Orionis cluster is stars located leftward (bottom panel) the photometric limit. We rejected as member the stars HD 36881 and HD 37148 which are located above the expected sequence. Large open circles represent stars with infrared excesses (see Section 3).

(A color version of this figure is available in the online journal.)

an aperture radius of 3″ and a background annulus from 3″ to 7″. Our estimation for HD 245168 indicates 2MASS photometry of $J = 9.50$, $H = 9.52$, and $K = 9.45$ with a photometric error of 5%; we added this star to our preliminary sample. Using the Kharchenko (2001) catalog (limiting magnitude of $V = 12$–14) and visual inspection on the IRAC 3.6 μm image, we did not find additional bright stars not included in the 2MASS catalog.

Figure 1 illustrates the procedure to select early-type candidates (F5 or earlier) of the λ Orionis cluster. The NIR color–color diagram (upper left panel) for the preliminary sample reveals that most of the stars are located on the main-sequence locus (Bessell & Brett 1988) indicating that, in general, these stars have little extinction and no NIR excesses. Only two stars appear to have large extinction or NIR excesses. One star (HD 245185; V1271 Ori), a well-known Herbig Ae star with spectral type A5 (e.g., Wade et al. 2007; Acke et al. 2005; Hernández et al. 2004; de Winter et al. 2001; Herbst & Shevchenko 1999; Finkenzeller & Mundt 1984), appears in the HAeBe star loci (Hernández et al. 2005), where the NIR excess can be explained by emission from an optically thick primordial disk with a sharp dust–gas transition at the dust destruction radius (Dullemond & Dominik 2004). The other star (HD 36881) is a spectroscopic binary with a peculiar spectral type B9III (Pedoussaut et al. 1988). Since HD36881 does not lie near the zero-age main sequence (ZAMS; even allowing for photometric errors or binarity), probably this star is a foreground nonmember (Dolan & Mathieu 2001; see also lower panel of Figure 1). The dotted horizontal line in the NIR color–color diagram is the $[J-H]$ limit corresponding to a F5 star with $A_V = 0.4$. We identified 35 early-type candidates located below this limit. We also included the Herbig Ae (HAe) star HD245185 as a early-type star of the λ Orionis cluster.

The upper right panel shows the vector point diagram for the early-type candidates. Proper motions are from Röser et al. (2008). In this panel, we also show distributions of proper motions which can be represented by Gaussians centered at $\mu_\alpha * \cos(\delta) \sim 0.0$ mas yr^{-1} and $\mu_\delta \sim 0.3$ mas yr^{-1}, with $\sigma = 2.5$ mas yr^{-1}. Most of the stars are located in a well-defined region represented for the 3σ criteria circle in the vector point plot; however, the proper motion of the star λ Orionis does not agree with the general trend of the cluster. To explain these peculiar proper motions (as other peculiar kinematic properties), several authors (e.g., Maddalena & Morris 1987; Cunha & Smith 1996; Dolan & Mathieu 1999) have invoked the presence of a massive companion of the λ Orionis star that became a supernova (SN), affecting the λ Orionis's kinematics and removing nearby molecular gas at the center of the cluster about 1 Myr ago when the SN exploded (Dolan & Mathieu 2001). If this scenario is correct, then the SN explosion may have affected the kinematics of other members of the cluster specially if those members were part of a multiple system, λ Orionis + SN, or were still in formation and embedded in their molecular cloud. So we cannot use kinematic properties alone as a reliable criteria for membership.

The lower panel in Figure 1 shows the color–magnitude diagram, V versus $V-J$, for the early-type candidates. Most stars are located near or in the region defined by the ZAMS and the 5 Myr isochrone (Siess et al. 2000). Since it is well known that theoretical isochrones not including the birth line do not accurately match empirical isochrones for intermediate-mass stars (Hartmann 2003), and theoretical evolutionary models often ignore some hydrodynamic processes in stellar models (Mamajek et al. 2008), these theoretical isochrones are plotted as reference only and are not used for our selection of the photometric candidates. However, comparing empirical isochrones in the low-mass star range, we showed that the λ Orionis cluster is in similar evolutionary stage as other groups with ages quoted as 5 Myr (Hernández et al. 2008), which is in agreement with previous results (e.g., Barrado y Navascués et al. 2007; Dolan & Mathieu 2002). Two stars (HD36881 and HD37148) are located above the general trend described by the sample. The star HD36881 was reported previously as a foreground star (Dolan & Mathieu 2001) as discussed above, and HD37148 has the largest proper motion of the sample ($\mu_\delta = -33.5$ mas yr^{-1}; see the upper right panel), even larger than the proper motion of the star λ Orionis. We excluded those two stars from being members of the cluster. In this contribution, we also excluded stars located rightward from the dotted line, which represents the limit corresponding to a F5 star with $A_V = 0.4$. Our final sample includes 29 early-type candidates of the λ Orionis cluster.

Stars with detected infrared excesses (see Section 3) are encircled in the lower panel of Figure 1. Optical spectra were obtained for these stars using the 1.3 m McGraw-Hill Telescope of the MDM Observatory equipped with the Boller & Chivens CCD spectrograph (CCDS). We used the 150 grooves per mm grating centered at 5300 Å. This configuration provides a

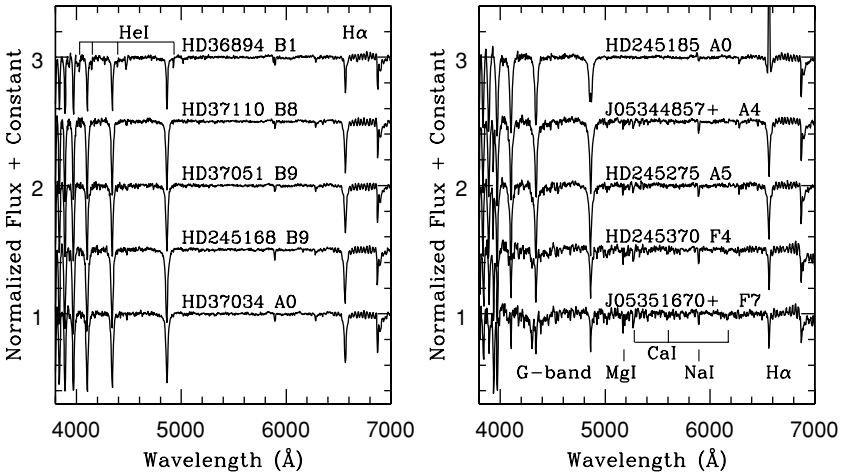

Figure 2. Optical spectra of the intermediate-mass stars bearing disks sorted by spectral types. The spectra were obtained with the CCDS spectrograph on the 1.3 m telescope of the MDM Observatory. Spectral types were obtained using the SPTCLASS code, some features used for spectral classification are marked in the panels. Emission lines are detected only in the HAe star HD 245185.

nominal resolution of ∼5 Å with spectral coverage from 3800 Å to 7100 Å. In Figure 2, we show spectra for the stars with infrared excesses sorted by spectral types. Spectral types were obtained using the SPTCLASS tool,[8] an IRAF/IDL code based on the methods described in Hernández et al. (2004). The HAe star HD 245185 shows emission lines suggesting that magnetospheric accretion processes are present in this star (Muzerolle et al. 2004). The other stars do not show emission lines in their optical spectra indicating that magnetospheric accretion has stopped; this characteristic is typically observed in diskless stars and stars bearing debris disks. Most stars not observed with the CCDS have spectral types from Cannon & Pickering (1993). For the stars without spectral type information, we estimated the latest spectral type they may have by assuming no reddening and interpolating the observed $V-J$ color in the table of standard colors given by Kenyon & Hartmann (1995).

Table 1 shows optical and *Spitzer* data for the early-type candidates. Columns 1 and 2 show the name and the 2MASS denomination of the stars. Columns 3–6 show the IRAC magnitudes. Column 7 shows the 24 μm MIPS fluxes. The typical errors in the IRAC and MIPS magnitudes are 0.02–0.05 and 0.03–0.06, respectively. Column 9 shows the excess ratio of the measured flux at 24 μm from that expected from the stellar photosphere (see Section 3). Spectral types and references are in Columns 10 and 11. Visual magnitudes and references are in Columns 12 and 13. The last column shows the disk type around each star (see Sections 3 and 4).

3. DISK DIAGNOSTIC

3.1. Identifying Stars with Infrared Excess

To characterize the disk population among stars of the λ Orionis cluster, we need to identify photometric candidates that exhibit excess emission at the IRAC/MIPS bands. Since a disk produces greater excess emission above the stellar photosphere at longer wavelengths, we selected the bands at 8 μm and 24 μm to identify stars with infrared emission due to the presence of disks. First, we identified stars with 24 μm infrared excess above the photospheric level in the upper panel of Figure 3. In the upper portion of this panel, we plot the $K-[24]$ color distribution for the sample. The distribution of stars around

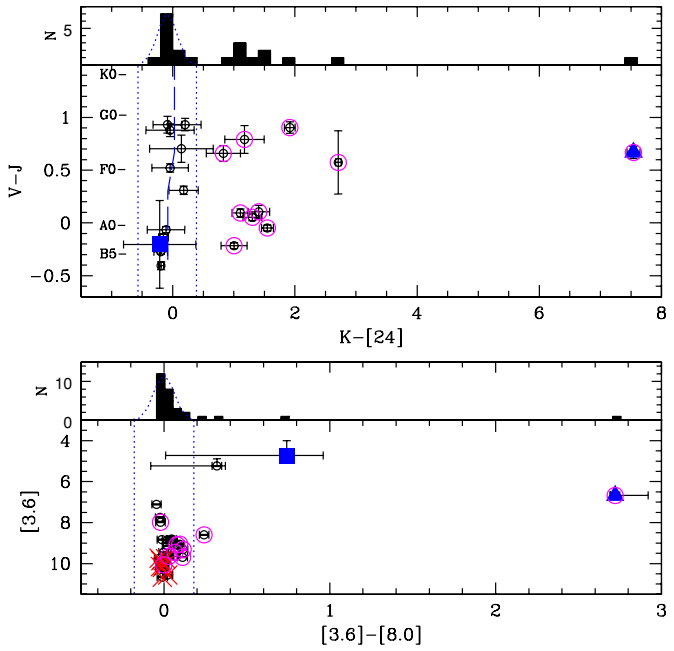

Figure 3. $V-J$ vs. $K-[24]$ color–color diagram for intermediate-mass stars in the λ Orionis cluster (upper panel). Dotted lines define the locus expected for diskless stars based on the $K-[24]$ color distribution. Nine stars exhibit moderate excess at 24 μm ($K-[24] < 3$) while the HAe star (HD 245185: triangle) exhibits strong excess at 24 μm ($K-[24]$ ∼7.5). The bottom panel shows the color–magnitude diagram, [3.6] vs. [3.6]–[8.0], used to detect stars with excess at 8 μm. Dotted lines define the photospheric limit based on the [3-6]–[8.0] color distribution. The two brightest stars in this plot are affected by saturation at 3.6 μm. Since these stars do not show excess at 24 μm, the excess detected at 8 μm is not real. Thus, in addition to the HAe star (triangle), we have detected one star with small excess at 8 μm (HD 245370). The square represents the central star λ Orionis.

(A color version of this figure is available in the online journal.)

the expected photospheric color ($K-[24] \sim 0$) describes a Gaussian centered at $K-[24] = -0.09$ with $\sigma = 0.16$. The 3σ boundaries (vertical dotted lines) represent the photospheric colors; thus stars with excess at 24 μm have colors $K-[24] > 0.4$. Besides the HAe star, which displays the largest excess at 24 μm in our sample, we detected nine stars (hereafter debris disk candidates) with varying degree of 24 μm excesses comparable to the debris disk population in other young stellar

[8] http://www.astro.lsa.umich.edu/∼hernandj/SPTclass/sptclass.html

Table 1
Early-type Stars of the λ Orionis Cluster

ID	2MASS	[3.6] (mag)	[4.5] (mag)	[5.8] (mag)	[8.0] (mag)	$F_{24\,\mu m}$ (mJy)	Excess Ratio	Spectral Type	Reference	V mag	Reference	Disk Type
HD36861	05350831+0956036	4.728	4.381	4.006	3.988	169.31	0.89	O5	2	3.532	4	No disk
HD36822	05344923+0929225	5.235	5.002	4.994	4.916	69.81	0.91	B0	2	4.402	4	No disk
HD36895	05351280+0936478	7.114	7.163	7.146	7.159	9.01	0.91	B3	2	6.722	4	No disk
HD245203	05351380+0941494	7.741	7.749	7.733	7.765	5.49	0.94	B8	2	7.465	4	No disk
HD36894	05351670+0946394	7.982	7.978	7.973	8.003	12.28	2.74	B2	1	7.614	4	Debris
HD37035	05355825+0931541	8.852	8.795	8.785	8.833	2.04	0.98	B9	2	8.638	4	No disk
HD37110	05362962+0937542	9.055	9.082	9.075	8.960	7.34	4.53	B8	1	8.944	4	Debris
HD37051	05360418+0949550	9.087	9.045	9.039	9.009	4.97	3.01	B9	1	9.087	4	Debris
HD245140	05345817+0956267	8.803	8.772	8.740	8.757	2.67	1.28	B9	2	9.218	4	No disk
HD37034	05355938+0942480	9.311	9.271	9.300	9.196	4.70	3.61	A0	1	9.335	4	Debris
HD37159	05365811+1016586	8.849	8.787	8.781	8.796	2.11	1.05	A3	2	9.427	4	No disk
HD245168	...	9.452	9.459	9.420	9.385	4.44	3.98	B9	1	9.605	4	Debris
HD245185	05350960+1001515	6.679	6.201	5.498	3.958	4702.13	1129.9	A0	1	9.959	4	Primordial
HD245370	05360940+1001254	8.599	8.557	8.543	8.357	14.27	6.35	F4	1	10.014	4	Debris
HD244927	05335042+1004211	8.828	8.829	8.841	8.841	2.44	1.31	A7	2	10.163	4	No disk
HD244907	05335115+0946421	9.139	9.108	9.172	9.120	1.53	1.04	F8	2	10.357	4	No disk
HD244908	05334712+0940261	9.760	9.772	9.787	9.751	...	...	A2	2	10.361	4	No disk
...	05344857+0930571	9.694	9.631	9.634	9.582	11.38	12.46	A4	1	10.437	5	Debris
HD245275	05354485+0955243	9.648	9.553	9.604	9.619	2.13	2.33	A5	1	10.463	4	Debris
HD245385	05361338+0959244	9.653	9.626	9.637	9.630	1.13	1.24	A0	2	10.536	4	No disk
...	05335032+0958185	9.439	9.447	9.451	9.441	1.14	1.00	F7	3	10.699	4	No disk
HD245386	05362132+0950414	9.745	9.720	9.716	9.774	...	...	A2	2	10.924	5	No disk
...	05345914+0933508	10.143	10.172	10.181	10.164	...	...	F3	3	11.036	5	No disk
299-3	05360529+1021271	10.190	10.185	10.196	10.201	...	...	F3	3	11.082	4	No disk
...	05365226+0929584	9.862	9.856	9.864	9.881	...	...	F9	3	11.174	4	No disk
...	05352468+1011452	10.070	10.085	10.106	10.071	1.98	3.21	F7	1	11.254	4	Debris
...	05334028+0948013	10.103	10.096	10.092	10.104	...	...	F6	3	11.265	4	No disk
h-star	05350920+1002518	10.670	10.637	10.703	10.680	...	...	F8	3	11.999	5	No disk
...	05354220+1013447	10.560	10.538	10.540	10.537	...	...	G0	3	12.022	5	No disk

References. (1) Cannon & Pickering 1993; (2) This work; (3) Photometric spectral types; (4) Kharchenko 2001; (5) Dolan & Mathieu 2002.

regions (e.g., Young et al. 2004; Hernández et al. 2006; Gorlova et al. 2007; Currie et al. 2008a, 2008b), and with no emission lines in their optical spectra (see Figure 2). As reference, we displayed the location of the spectral type sequence, using the standard $V-J$ colors from Kenyon & Hartmann (1995), and the corresponding $K-[24]$ photospheric colors from the STARPET tool of the Spitzer Science Center.[9]

The lower panel of Figure 3 shows the [3.6]–[8.0] color–[3.6] magnitude diagram illustrating the procedure to detect infrared excess at 8 μm. The photospheric limits are defined using 3σ criteria based on the [3.6]–[8.0] color distribution, which can be represented by a Gaussian centered at [3.6]–[8.0] ~ 0 with $\sigma = 0.06$. The error bars include the saturation effect; that were estimated using the deviation from the expected photospheric colors for the brightest objects detected in each IRAC band. Thus, the apparent 8 μm excess observed in stars with [3.6] $<$ 6 mag is produced by saturation effect in the [3.6] band. Besides the HAe star which displays excesses in all IRAC bands, the star HD 245370 shows small excess at 8 μm; this star also shows the third largest excess at 24 μm ($K-[24] \sim 2$).

3.2. Spectral Energy Distributions

We have plotted the spectral energy distributions (SEDs) for the disk-bearing stars found in our early-type sample of the λ Orionis cluster. Figure 4 shows the SEDs for the Herbig Ae star HD 245185 and for the debris disk candidates sorted by spectral types. The color excess, E_{V-J}, was calculated using the observed $V-J$ color and the standard color obtained interpolating the spectral type (see Section 2.2) in the calibration given by Kenyon & Hartmann (1995). Using the E_{V-J} and the extinction relation for normal interstellar reddening (Cardelli et al. 1989), we obtained the visual extinctions reported in Figure 4. Since the J magnitude of the HAe star could have contribution from the disk, we calculate the A_V for this star using the $B-V$ color from Kharchenko (2001). Out of 10 stars plotted in Figure 4, two stars (20%) have A_V larger than the value used as cutoff in Section 2.2 ($A_V = 0.4$). Since stars bearing disks are expected to have larger extinctions produced by the circumstellar material, we can estimate that the completeness in our selection of stars earlier than F5 is larger than 80%. A F0 star needs to have $A_V > 0.8$ to be rejected from our sample (see Figure 1).

Dotted lines in these plots represent the standard colors (or photospheric levels) for a given spectral type (Kenyon & Hartmann 1995). Figure 4 also shows the excess ratio at 24 μm (Rieke et al. 2005), which was calculated using the relation: $E_{24} = 10^{0.4*(K-[24]+0.09)}$, where -0.09 is the median value of $K-[24]$ for the photometric candidates with MIPS detections (see Section 3.1). In summary, we detected 10 early-type disk-bearing stars in the λ Orionis cluster. The HAe star HD 245185 is the only star that shows infrared excesses in all the *Spitzer* bands, in agreement with the presence of a primordial optically thick disk; emission lines in its optical spectrum indicates that HD 245185 is accreting material from the disk to the star. Only the debris disk candidate HD 245370 shows infrared excess at

[9] http://ssc.spitzer.caltech.edu/tools/starpet/

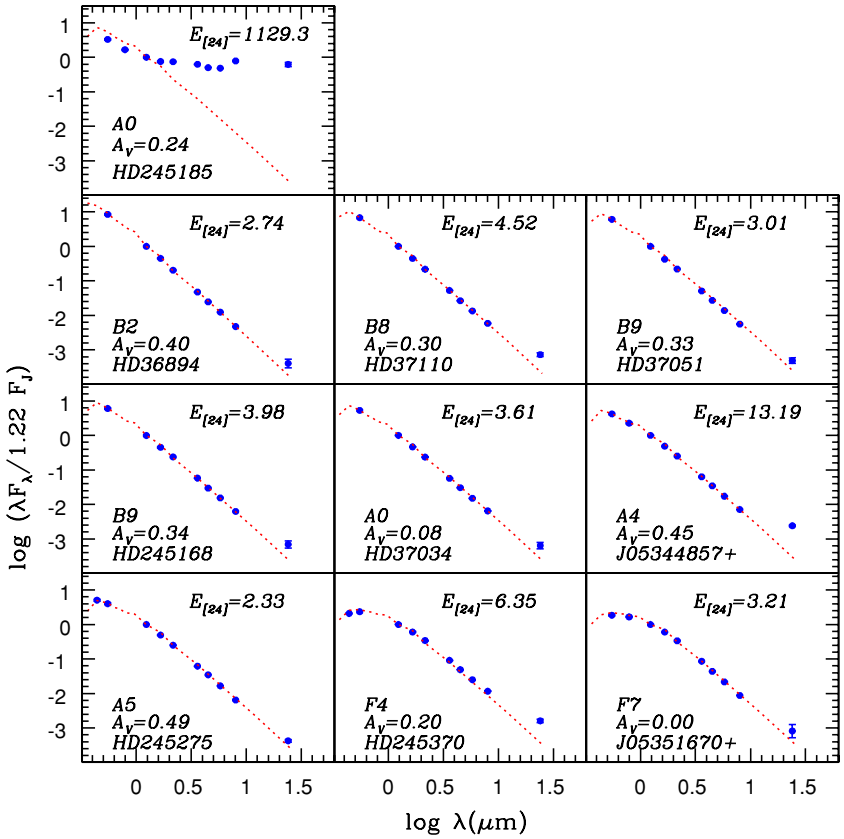

Figure 4. Spectral energy distributions for intermediate-mass stars with infrared excess. Each panel shows the spectral type of the object (see Section 2.2), and the excess ratio, E24 (Rieke et al. 2005), calculated from the $K - [24]$ color. Dotted lines show the corresponding photospheric colors (Kenyon & Hartmann 1995). Except for the star HD 245185, A_V's were calculated using the $V - J$ color. Since the J magnitude of HD 245185 can be contaminated by disk emission, we have used the color $B - V$ to calculate the reddening in this HAe star. All SEDs are corrected by reddening and normalized at the J band.

(A color version of this figure is available in the online journal.)

8 μm, the remaining debris disk candidates only exhibit infrared excess at 24 μm.

4. DEBRIS DISK FREQUENCY IN YOUNG STELLAR POPULATIONS

In Hernández et al. (2006), we reported that debris disks in the range of ages from 2.5 to 150 Myr are more frequent and have larger 24 μm excess around 10 Myr. This peak in the debris disk phenomenon is in agreement with models of evolution of solids in the region of the protoplanetary disk where icy planets are predicted to form (30–150 AU; Kenyon & Bromley 2004, 2005, 2008). Observational results from the double cluster h and χ Persei (10–15 Myr; Currie et al. 2008b), and the cluster NGC2232 (25 Myr; Currie et al. 2008a) support our finding. However, it is still an open question whether the disk emission observed at 24 μm in debris disks candidates younger than 10 Myr originates from remaining primordial dust or from second generation dust produced by collisional cascades in the disk (e.g., Hernández et al. 2006; Hillenbrand 2008; Wyatt 2008; Cieza 2008). To tackle this question, we have compared the disk population in the λ Orionis cluster to disk populations of several stellar groups located within 500 pc of the Sun detected and characterized with the same methods (Hernández et al. 2006, 2007a, 2007b, 2008; J. Hernández et al. 2010, in preparation).

Figure 5 shows the theoretical stellar fluxes at 24 μm for diskless stars in the stellar populations of Table 2. Using the Siess et al. (2000) evolutionary tracks and the properties listed in Table 2, we estimated the apparent K magnitude for stars in each stellar group. The 24 μm fluxes were calculated using the corresponding $K - [24]$ photospheric colors obtained from the STAR-PET tool of the Spitzer Science Center and the zero-point magnitude defined for MIPS observations ($\sim$7.17 Jy[10]). Given the limiting flux at 24 μm (0.5–0.7 mJy), and using the Siess et al. (2000) evolutionary tracks to estimate the K magnitude for stars in each stellar group, we inferred that we can detect any excess at 24 μm in stars F0 or earlier with low or moderate reddening. Figure 5 shows the limit for diskless stars ($E_{24} = 1$). The detection thresholds at 24 μm for intermediate-mass stars in different clusters are given by the width of the photospheric region defined by the $K - [24]$ color distributions. These detection thresholds are nearly the same in all stellar populations of Table 2, in which we can detect 24 μm excess in intermediate-mass stars with $E_{24} > 1.6$. We also show in Figure 5 the detection threshold for stars bearing disks with $E_{24} = 5$. Figure 5 indicates that for all our surveys the spectral type limit for detecting stars bearing disks with $E_{24} \geqslant 5$ is M1 $\pm$ 1.

Using the same method for 8 μm, we estimated that a diskless star in our surveys with spectral type M5 has [8.0] $<$ 13. This is well above of the IRAC detection limits of our surveys ([8.0] $\sim$ 14.0–14.5). The detection threshold at 8 μm for a M5 star is defined by the error of the IRAC SED slope. The IRAC SED slope, used to identify infrared excess at 8 μm in low-mass stars, is calculated from the [3.6]–[8.0] color and its error is dominated by the photometric error at [8.0]. Thus, using

[10] http://ssc.spitzer.caltech.edu/mips/calib/

Table 2
Properties of Stellar Populations

Name	Distance (pc)	Reference	A_V (mag)	Reference	Age (Myr)	Reference	$E_{24} \geqslant 5$[a] (SpT)
σ Ori	440	1,2	0.2	9,10	2–4 Myr	2	M2
λ Ori	450	3,4	0.4	11	5 Myr	4	M0
Ori OB1b	440	5	0.4	5	5 Myr	5	M0
γ Vel	350	6,7,8	0.2	12,13	5–7 Myr	13	M2
Ori OB1b	330	5	0.3	5	8–10 Myr	5	M1

Note. [a] The last column represents the later spectral type in which we can detect infrared excess at 24 μm with $E_{24} \geqslant 5$ (see Figure 5).

References. (1) Brown et al. 1998; (2) Sherry et al. 2008; (3) Dolan & Mathieu 2001; (4) Mathieu 2008; (5) Briceño et al. 2007; (6) van Leeuwen 2007;(7) Millour et al. 2007; (8) North et al. 2007; (9) Brown et al. 1994; (10) Béjar et al. 1999; (11) Diplas & Savage 1994;(12) Pozzo et al. 2000; (13) Jeffries et al. 2009.

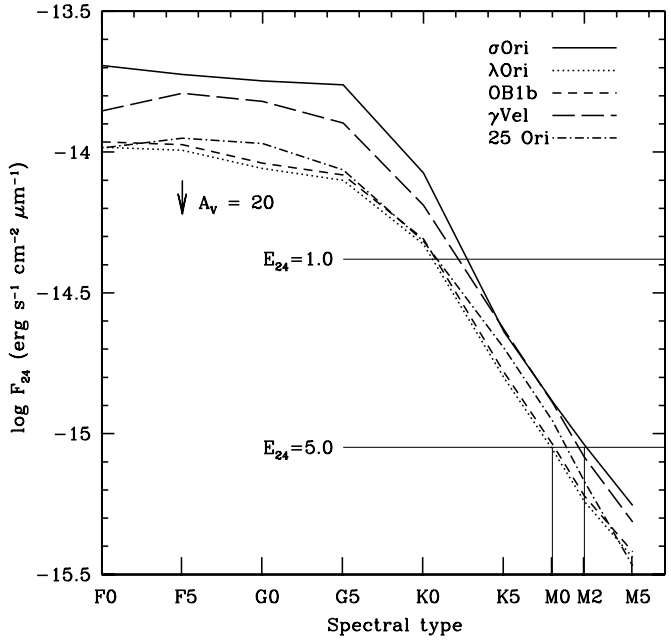

Figure 5. Theoretical stellar fluxes at 24 μm. Combining the Siess et al. (2000) evolutionary tracks and the corresponding $K - [24]$ photospheric colors from STAR-PET tool of the Spitzer Science Center we estimated the theoretical flux expected for the stellar populations with distances, ages, and extinctions listed in Table 2. Given the limiting flux at 24 μm (0.6–0.7 mJy), we plotted the limit where we can detect any excess at 24 μm ($E_{24} = 1$). For reference, we also plotted the limit where we can detect stars bearing disks with $E_{24} \geqslant 5$. Vertical thin lines define the spectral type range in which we can detect stars bearing disks with $E_{24} \geqslant 5$. The arrow represents reddening vector of $A_V = 20$.

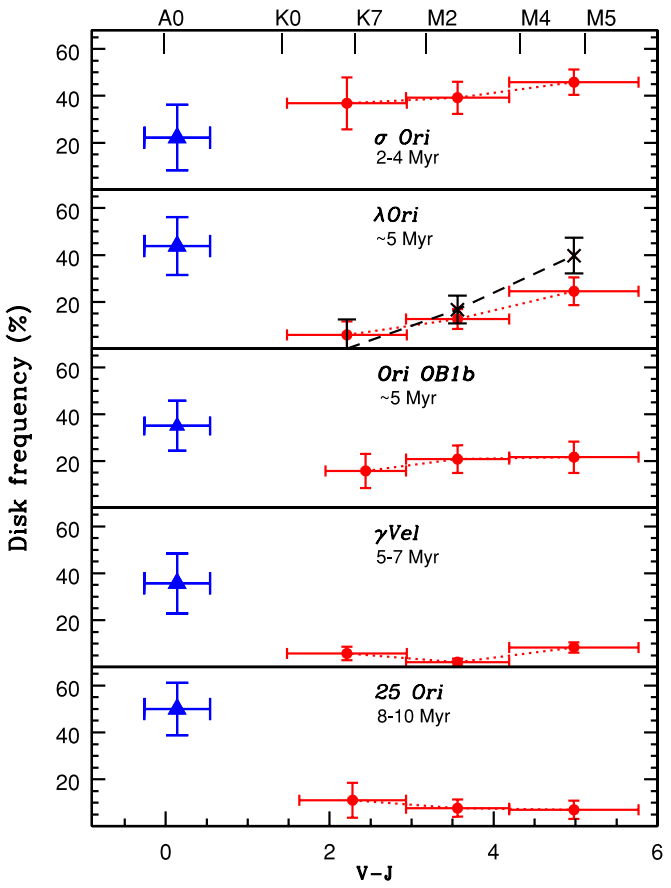

Figure 6. Disk frequency vs. spectral types for several star-forming regions. In the stellar population of 3 Myr, disk frequencies for A-type stars are lower than disk frequencies around low-mass stars in agreement with the expected trend for primordial disk dissipation. In contrast, at 5 Myr and older, disks around A-type stars are more frequent than in low-mass stars indicating that second generation dusty disk must dominated the disk population at higher stellar masses. The low-mass bins are centered at the spectral types K6.5, M2.5, and M4.5. Using these values we calculated a reference detection threshold for each bin (see Figure 5): $E_{24} \sim 3, 7, 10$ (from left to right). The detection threshold for the intermediate-mass bin is given by the width of the photospheric region in each stellar group (e.g., Figure 3), $E_{24} \sim 1.6$. For the λ Orionis cluster, we plotted with "X"'s the disk frequencies calculated from the disk census in Barrado y Navascués et al. (2007). Since the IRAC thresholds defined in Barrado y Navascués et al. (2007) do not include photometric errors, the number of disk-bearing stars in the last bins could be overestimated.

(A color version of this figure is available in the online journal.)

the typical error in the IRAC SED slope at [8.0] = 13 (∼0.25 for all surveys), we can detect disks around stars with spectral type M5 or earlier with a excess ratio at 8 μm larger than 1.2.

Figure 6 shows observed disk frequencies as a function of color/spectral type for several young stellar populations, the clusters σ Ori, λ Orionis, γ Velorum, a region in the Orion OB1b subassociation, and the stellar aggregate 25 Ori. Frequencies were calculated for several bins of spectral types in each stellar population.

The bin corresponding to the intermediate-mass stars includes stars ranging from B8 to F0; most of the intermediate-mass stars with infrared excesses are in this range (Hernández et al. 2006, 2007a, 2008). In general, the intermediate-mass stars of the stellar populations plotted in Figure 6 have spectral type information available in the literature (Houk 1978; Houk & Swift 1999; Nesterov et al. 1995; Kharchenko 2001; Caballero 2007; Hernández et al. 2005, 2006); optical photometric colors were used to estimate spectral types for stars without spectral type information. In agreement with the extinctions listed in

Table 2, the reddening for intermediate-mass stars in these stellar groups is relatively low. Except for the star HD36219 located in the Orion OB1b subassociation (with $A_V = 1.46$), all stars in the intermediate-mass samples plotted in Figure 6 have $A_V < 1$.

Disks around low-mass stars were split in three bins of spectral types: from K0.5 to M0.5, from M0.5 to M3.5 and from M3.5 to M6 (hereafter the low-mass bins). Given the low reddening expected for the stellar populations plotted in Figure 6, photometric colors represent a good approximation of spectral types when spectroscopic information is not available for the stellar groups. Thus, we used the standard table of colors given by Kenyon & Hartmann (1995) to obtain spectral type estimations. Observed disk frequencies of low-mass stars in the λ Orionis cluster were calculated analyzing the IRAC and MIPS photometry of members confirmed spectroscopically by Dolan & Mathieu (2001); Barrado y Navascués et al. (2007); Maxted et al. (2008), and Sacco et al. (2008) using radial velocity distributions and the presence of Li I in absorption (J. Hernández et al. 2010, in preparation). *Spitzer* point-source photometry for these low-mass members was obtained using the same methods described in Section 2.1. Disk detection follows the method described in Hernández et al. (2007a, 2007b, 2008). We used NIR photometry from the 2MASS catalog (Cutri et al. 2003) and optical photometry from Dolan & Mathieu (2002) and Barrado y Navascués et al. (2007). Since the $R-J$ color is more complete for the spectroscopic members compiled for the λ Orionis cluster, we used this color to calculate photometric spectral types and separate the sample in the bins described above. For comparison, we plotted the disk frequencies obtained from the disk census in Barrado y Navascués et al. (2007). Since the IRAC photospheric region defined in Barrado y Navascués et al. (2007) does not take into account photometric errors, the number of stars bearing disks could be overestimated in the lowest mass bins (M. Morales-Calderon 2009, private communication).

For the σ Orionis cluster, we used the disk census in Hernández et al. (2007a). To reduce the contamination by nonmembers, observed disk frequencies of low-mass stars were calculated using the spectroscopic members compiled in Hernández et al. (2007a), members confirmed by Sacco et al. (2008) and Maxted et al. (2008), and the X-ray members from Franciosini et al. (2006). Since most of this sample does not have spectral types, we used the color $V-J$ in Hernández et al. (2007a) and the standard colors (Kenyon & Hartmann 1995) to separate the low-mass sample in the low-mass bins.

For the Orion OB1b subassociation and the 25 Orionis aggregate we used the disk census in Hernández et al. (2007b). Observed disk frequencies were calculated using confirmed members and spectral types calculated using our SPTCLASS code (Briceño et al. 2005, 2007; C. Briceño et al. 2010, in preparation). Since our samples of confirmed members in the Orion OB1b subassociation and the 25 Orionis do not go as early as K0.5, the first low-mass star bin in these groups does not cover the same spectral type range as the other stellar populations in Figure 6 (from K2 for the 25 Orionis aggregate and from K4 for the Orion OB1b subassociation).

Finally, for the γ Velorum cluster we used the disk census in Hernández et al. (2008). Observed disk frequencies were calculated using the number of members expected as a function of $V-J$ color (Hernández et al. 2008); this color was used to separate the sample in the low-mass bins. Using empirical Li-depletion studies and empirical isochrone comparisons, the γ Velorum cluster appears to be slightly older than the λ Orionis cluster (5–7 Myr; Jeffries et al. 2009) and younger than the 25 Orionis stellar aggregate (Hernández et al. 2008).

In Figure 6, the observed disk frequencies in the low-mass stars bins were calculated using the infrared excess at 8 μm. Since a disk produces greater emission above the stellar photosphere at longer wavelengths, those stars with excess at 8 μm are expected to have excess at 24 μm. However, since the sensitivity of the 24 μm MIPS band is lower than that of the IRAC 8 μm channel, some of the faintest stars bearing disks are below the MIPS detection limit. We also included as stars bearing disks, stars with small or no infrared excesses in the IRAC bands but detectable excess at 24 μm (transitional disk candidates). The transitional disk candidates represent a relative small fraction of the disk-bearing stars in these stellar groups ($\lesssim$10%; Hernández et al. 2007b; Ercolano et al. 2009; Uzpen et al. 2009), so they do not significantly affect our conclusions.

The infrared excesses observed in low-mass stars are unlikely from second generation dust. *Spitzer* observations of 314 solar-type stars[11] in the Formation and Evolution of Planetary Systems (FEPS) Legacy program (Carpenter et al. 2009) indicate that the dust temperature of debris disks ($T_{\rm dust}$) ranges from ∼50 K to ∼200 K, with a fractional dust luminosity ($f_{\rm dust} = L_{\rm dust}/L_*$) less than 10^{-3}. Adopting these values, following the two-parameter model of Wyatt (2008), and using the stellar parameters for a K0 star at 3, 5, and 10 Myr (Siess et al. 2000), we estimated that debris disks around low-mass stars show small or no excess at 8 μm ($E_8 < 1.2$) and modest excess at 24 μm ($E_{24} < 4$). The two-parameter model includes two fundamental observable parameters of debris disks ($T_{\rm dust}$ and $f_{\rm dust}$) and it is useful to estimate the expected infrared excesses produced by a second generation disk with a unique $T_{\rm dust}$; however, note that we need a more detailed model to reproduce the SED that for some disks can only be explained by the presence of several dust populations with different temperatures. In general, low-mass stars bearing disks in our census show excesses much larger than those expected for debris disks ($E_{24} > 25$), thus the low-mass bins in Figure 6 represent frequencies of primordial disks with little or no contamination by second generation dust.

In contrast, the two-parameter model (Wyatt 2008) applied to debris disks around A0 stars with dust temperatures ranging from 50 K to 200 K and fractional luminosity of 10^{-3} indicates maximum E_{24} values of 29, 21, and 21 at ages of 3, 5, and 10 Myr, respectively. In general, debris disks around intermediate-mass stars exhibit less infrared excess than these maximum levels (e.g., Rieke et al. 2005; Hernández et al. 2006; Currie et al. 2008b; Wyatt 2008). Studying the MIPS observations of 160 A-type stars (with age range from 5 Myr to 850 Myr), Su et al. (2006) showed that debris disk systems have $f_{\rm dust} < 10^{-3}$ and most of them (> 90%)are characterized by dust temperatures between 50 K and 200 K (although for stars older than 400 Myr the dust temperatures of the disks appear in a narrow range between 50 and 150 K). Since our debris disks candidates have similar levels of 24 μm excess than those reported in older debris disks systems (e.g., Rieke et al. 2005; Su et al. 2006; Gorlova et al. 2007; Currie et al. 2008b), we expect a similar range of $T_{\rm dust}$ and $f_{\rm dust}$. Debris disks with $T_{\rm dust} \geqslant 200$ K (and/or $f_{\rm dust} \geqslant 10^{-3}$) are very scarce (Zuckerman & Song 2004; Williams & Andrews 2006; Su et al. 2006; Bryden et al. 2006; Rhee et al. 2007; Wyatt 2008; Uzpen et al. 2009). This kind of massive debris disks (like HR4796A and β Pic) can be above our estimations of E_{24} and could be explained if the observed dust is produced by eventual collisions between two large objects (>1000 km; Kenyon &

[11] Ranging in spectral types from late F to early K and in the range of ages from 3 Myr to 3 Gyr.

Bromley 2004, 2005; Song et al. 2005). However, an alternative explanation is that those objects are in a phase between HAeBe star and true debris systems (Rieke et al. 2005) retaining some of the primordial dust. The star HD245370 shows excess at 8 μm that can be explained by the two-parameter model assuming a $T_{\rm dust} \sim 250$ K; however, this star is outside of the intermediate-mass bin plotted in Figure 6. In our samples of intermediate-mass stars, only three stars bearing disks show excess at 24 μm larger than the theoretical limits calculated above: HD 290543 in the Orion OB1b subassociation ($E_{24} = 537.5$), HD 245185 in the λ Orionis cluster ($E_{24} = 1129.3$), and V346 Ori in the 25 Orionis aggregate ($E_{24} = 376.4$). These three stars also show Hα in emission indicating the presence of an accreting primordial disk. The remaining intermediate-mass stars with disks exhibit characteristics normally present in debris disk systems; they have $E_{24} < 12.5$ and no emission lines in their optical spectra.

In summary, in the low-mass bins the detection threshold is such that only primordial disks can be detected. In contrast, both primordial disks and debris disks can be detected in the intermediate-mass bin. We may take then the observed frequency of disks in the low-mass bins in Figure 6 as an indicator of the frequency of primordial disks. Figure 6 shows that the observed disk frequencies in K and M stars decrease as the stellar groups become older. Previous studies have shown that in young stellar populations primordial disks dissipate faster with higher stellar masses, for instance, in IC348 (2–3 Myr; Lada et al. 2006; Currie & Kenyon 2009), NGC 2264 (∼3 Myr; Sung et al. 2009), and σ Ori in Figure 6. According to this trend, the frequency of primordial disks around intermediate-mass stars should decrease with age in proportion to the observed decrease in the primordial disk frequency in the low-mass bins. However, Figure 6 shows that the observed frequency of disks in the intermediate-mass bin increases after ∼5 Myr. Since in this bin both primordial and debris disks can be detected, and since the primordial disk frequency is expected to decrease, the increase in disk frequency points to an increase in the frequency of debris disks. Assuming a binomial distribution for the errors of the disk frequencies, the significance of this increase ranges from 68%(1σ) to 95%(2.0σ). The increase in frequency of debris disks has been reported before by Hernández et al. (2006) and Currie et al. (2008a) at ∼10–15 Myr. The reversal in the observed disk frequency in the intermediate-mass bin shown in Figure 6 shows that this increase is already present at much earlier ages, at ∼5 Myr. Enough secondary dust must have been created by 5 Myr to make second generation dust detectable. This second generation dust must have been replenished from a reservoir, such as collisions between parent bodies (e.g., Chen 2006; Dominik & Decin 2003; Kenyon & Bromley 2004).

Kenyon & Bromley (2008) described a suite of numerical calculations of planets growing from ensembles of icy planetesimals at 30–150 AU in disks around 1–3 $M_\odot$ stars. These models predict that the 24 μm excess from second generation dust rises at stellar ages of 5–10 Myr (during the transition from runaway to oligarchic growth, reaching sizes of ∼500 km), then peaks at 10–30 Myr (when the first objects reach their maximum size, ⩾1000 km) and finally slowly declines (as the reservoir of small solids in the disk diminishes). The expected theoretical trend has been observed previously by Hernández et al. (2006) and Currie et al. (2008b, 2009). However, Figure 6 suggests the second generation nature of the excesses observed at 24 μm in debris disk candidates of 5 Myr or older. Since evolutionary processes are expected to occur faster in the inner disk than the outer disks for primordial disks (Weidenschilling 1997; Dahm & Hillenbrand 2007; Lada et al. 2006; Sicilia-Aguilar et al. 2006) and for debris disks (Kenyon & Bromley 2004, 2005, 2008), there is a possibility that the debris disk candidates in our studies have an outer primordial disk component which does not contribute significantly to the emission observed at $\lambda \leqslant 24$ μm. An example of this kind of object is AU Mic, a ∼12 old M-type star with a collisional evolved debris region in the inner part of the disk, and with outer regions composed by pristine material that is still part of the remnant primordial disk (Metchev et al. 2005). Additional observations at longer wavelength or observation of gas component of the disk are needed to confirm the complete dissipation of the outer primordial disks in the young debris disks candidates. Finally, Currie & Kenyon (2009) suggested that debris disks can be present in the 2–3 Myr IC 348 cluster. Using theoretical models of dust removal (Takeuchi & Artymowicz 2001), they estimate that the dust removal timescale is less than 1/20 of the median age for IC 348 stars, even if there is some residual gas in an optically thin disk. Thus, we cannot reject the possibility that some of the disks detected around intermediate-mass stars of the σ Orionis cluster are second generation disks. We need additional studies to confirm the actual nature of the intermediate-mass stars bearing disks detected in this cluster.

5. SUMMARY AND CONCLUSIONS

We have used the IRAC and MIPS instruments on board the *Spitzer Space Telescope* to study the frequencies and properties of disks around the intermediate-mass population of the 5 Myr old λ Orionis cluster. We have selected 29 intermediate-mass stars (∼F5 or earlier) using optical and 2MASS photometry. One star, HD 245185, displays excesses in all IRAC band, strong excess at 24 μm and emission line in its optical spectra, supporting previous results in which HD 245185 is an HAe star having an accreting primordial disk (Finkenzeller & Mundt 1984; Herbst & Shevchenko 1999; de Winter et al. 2001; Hernández et al. 2004; Acke et al. 2005; Wade et al. 2007). Additionally, we have identified nine stars as debris disks, which exhibit modest excess at 24 μm and very small or no excesses in the IRAC bands. The SEDs of our debris disks sample are comparable to those observed in debris disk populations of older stellar groups. As expected in stars with second generation disks, these stars do not show detectable accretion indicators in their optical spectra.

We have combined observations of the λ Orionis cluster with those of other stellar groups of ages raging from 3 to 10 Myr located at < 500 pc from the sun, studied using similar methods to detect and characterize their disks. Because of observational thresholds, the disk frequencies observed in K and M stars reflect the primordial disk populations, while the observed disk frequencies in intermediate-mass stars encompass both primordial and debris disks. As expected in primordial disk evolution the observed frequencies in K and M stars are smaller in older stellar groups. However, observed disk frequencies in intermediate-mass stars, represented by a bin in spectral type from B8 to F0, show a behavior in sharp contrast with that expected for primordial disk evolution. In particular, the disk frequency in intermediate-mass star increases from ∼20% at ∼3 Myr, to ∼40% at 5 Myr, and to ∼50% at ∼10 Myr. Since the timescale for primordial disk dissipation is dependent on stellar mass, the expected frequency of primordial disks around intermediate-mass stars at ages ⩾ 5 Myr, as inferred from the corresponding frequency in low-mass stars, is very low. In stellar

population of 5 Myr or older, the observed disk frequencies in intermediate-mass stars are larger than in low-mass stars. Thus, the increasing in the observed disk frequency at these ages indicates that these disks are dominated by second generation dust. This result agrees with models of evolution of solids in the disks (Kenyon & Bromley 2008), in which at 5–10 Myr collisions start to produce copious amount of dust during the transition from runaway to oligarchic growth. When oligarchs reach sizes ∼500 km, collisions between 1–10 km objects produce debris instead of mergers and the leftover planetesimals are ground to dust.

We thank Thayne Currie and Maria Morales Calderon for insightful communications, and the anonymous referee for input that greatly improved this manuscript. This work is based on observations made with the *Spitzer Space Telescope* (GO-1 0037), which is operated by the Jet Propulsion Laboratory, California Institute of Technology under a contract with NASA. J.H. and N.C. gratefully acknowledge support from the NASA Origins program and the Spitzer General Observer program.

REFERENCES

Acke, B., van den Ancker, M. E., & Dullemond, C. P. 2005, A&A, 436, 209
Backman, D. E., & Paresce, F. 1993, in Protostars and Planets III, ed. E. H. Levy & J. I. Lunine (Tucson, AZ: Univ. Arizona Press), 1253
Barrado y Navascués, D., et al. 2007, ApJ, 664, 481
Béjar, V. J. S., Zapatero Osorio, M. R., & Rebolo, R. 1999, ApJ, 521, 671
Bessell, M. S., & Brett, J. M. 1988, PASP, 100, 1134
Briceño, C., Calvet, N., Hernández, J., Vivas, A. K., Hartmann, L., Downes, J. J., & Berlind, P. 2005, AJ, 129, 907
Briceño, C., Hartmann, L., Hernández, J., Calvet, N., Vivas, A. K., Furesz, G., & Szentgyorgyi, A. 2007, ApJ, 661, 1119
Brown, A. G. A., de Geus, E. J., & de Zeeuw, P. T. 1994, A&A, 289, 101
Brown, A. G. A., Walter, F. M., & Blaauw, A. 1998, arXiv:astro-ph/9802054
Bryden, G., et al. 2006, ApJ, 636, 1098
Caballero, J. A. 2007, A&A, 466, 917
Cannon, A. J., & Pickering, E. C. 1993, VizieR Online Data Catalog, 3135, 0
Cardelli, J. A., Clayton, G. C., & Mathis, J. S. 1989, ApJ, 345, 245
Carpenter, J. M., Mamajek, E. E., Hillenbrand, L. A., & Meyer, M. R. 2006, ApJ, 651, L49
Carpenter, J. M., et al. 2009, ApJS, 181, 197
Chen, C. H., et al. 2006, in ASP Conf. Ser. 352, New Horizons in Astronomy: Frank N. Bash Symposium, ed. S. J. Kannappan et al. (San Francisco, CA: ASP), 63
Cieza, L. A. 2008, in ASP Conf. Ser. 393, New Horizons in Astronomy: Frank N. Bash Symposium 2007, ed. A. Frebel et al. (San Francisco, CA: ASP), 35
Cox, A. N. 2000, Allen's Astrophysical Quantities (4th ed.; New York: Springer)
Cunha, K., & Smith, V. V. 1996, A&A, 309, 892
Currie, T., & Kenyon, S. J. 2009, AJ, 138, 703
Currie, T., Kenyon, S. J., Balog, Z., Rieke, G., Bragg, A., & Bromley, B. 2008a, ApJ, 672, 558
Currie, T., Lada, C. J., Plavchan, P., Robitaille, T. P., Irwin, J., & Kenyon, S. J. 2009, ApJ, 698, 1
Currie, T., Plavchan, P., & Kenyon, S. J. 2008b, ApJ, 688, 597
Cutri, R. M., et al. 2003, VizieR Online Data Catalog, 2246, 0
Dahm, S. E., & Hillenbrand, L. A. 2007, AJ, 133, 2072
de Winter, D., van den Ancker, M. E., Maira, A., Thé, P. S., Djie, H. R. E. T. A., Redondo, I., Eiroa, C., & Molster, F. J. 2001, A&A, 380, 609
Decin, G., Dominik, C., Waters, L. B. F. M., & Waelkens, C. 2003, ApJ, 598, 636
Diplas, A., & Savage, B. D. 1994, ApJS, 93, 211
Dolan, C. J., & Mathieu, R. D. 1999, AJ, 118, 2409
Dolan, C. J., & Mathieu, R. D. 2001, AJ, 121, 2124
Dolan, C. J., & Mathieu, R. D. 2002, AJ, 123, 387
Dominik, C., & Decin, G. 2003, ApJ, 598, 626
Duerr, R., Imhoff, C. L., & Lada, C. J. 1982, ApJ, 261, 135
Dullemond, C. P., & Dominik, C. 2004, A&A, 417, 159
Engelbracht, C. W., et al. 2007, PASP, 119, 994
Ercolano, B., Clarke, C. J., & Robitaille, T. P. 2009, MNRAS, 394, L141
Fazio, G. G., et al. 2004, ApJS, 154, 39
Finkenzeller, U., & Mundt, R. 1984, A&AS, 55, 109
Franciosini, E., Pallavicini, R., & Sanz-Forcada, J. 2006, A&A, 446, 501
Gordon, K. D., et al. 2005, PASP, 117, 503
Gorlova, N., Balog, Z., Rieke, G. H., Muzerolle, J., Su, K. Y. L., Ivanov, V. D., & Young, E. T. 2007, ApJ, 670, 516
Greenberg, R., et al. 1978, Icarus, 35, 1
Gutermuth, R. A., Megeath, S. T., Muzerolle, J., Allen, L. E., Pipher, J. L., Myers, P. C., & Fazio, G. G. 2004, ApJS, 154, 374
Haisch, K. E., Lada, E. A., & Lada, C. J. 2001, ApJ, 553, L153
Hartmann, L. 2003, ApJ, 585, 398
Hartmann, L., et al. 1998, ApJ, 495, 385
Herbst, W., & Shevchenko, V. S. 1999, AJ, 118, 1043
Hernández, J., Briceño, C., Calvet, N., Hartmann, L., Muzerolle, J., & Quintero, A. 2006, ApJ, 652, 472
Hernández, J., Calvet, N., Briceño, C., Hartmann, L., & Berlind, P. 2004, AJ, 127, 1682
Hernández, J., Calvet, N., Hartmann, L., Briceño, C., Sicilia-Aguilar, A., & Berlind, P. 2005, AJ, 129, 856
Hernández, J., Hartmann, L., Calvet, N., Jeffries, R. D., Gutermuth, R., Muzerolle, J., & Stauffer, J. 2008, ApJ, 686, 1195
Hernández, J., et al. 2007a, ApJ, 662, 1067
Hernández, J., et al. 2007b, ApJ, 671, 1784
Hillenbrand, L. A. 2008, Phys. Scr. T, 130, 014024
Houk, N. 1978 (ed.), Michigan Catalogue of Two-dimensional Spectral Types for the HD Stars, Vol. 2: Declinations −53.0 to −40.0 (Ann Arbor, MI: Department of Astronomy, Univ. Michigan), 12
Houk, N., & Swift, C. (ed.) 1999, Michigan Catalogue of Two-dimensional Spectral Types for the HD Stars, Vol. 5 (Ann Arbor, MI: Department of Astronomy, Univ. Michigan)
Jeffries, R. D., Naylor, T., Walter, F. M., Pozzo, M. P., & Devey, C. R. 2009, MNRAS, 393, 538
Kennedy, G. M., & Kenyon, S. J. 2009, ApJ, 695, 1210
Kenyon, S. J., & Bromley, B. C. 2004, AJ, 127, 513
Kenyon, S. J., & Bromley, B. C. 2005, AJ, 130, 269
Kenyon, S. J., & Bromley, B. C. 2008, ApJS, 179, 451
Kenyon, S. J., & Bromley, B. C. 2009, ApJ, 690, L140
Kenyon, S. J., & Hartmann, L. 1995, ApJS, 101, 117
Kharchenko, N. V. 2001, Kinematika Fiz. Nebesnykh Tel, 17, 409
Lada, C. J., et al. 2006, AJ, 131, 1574
Maddalena, R. J., & Morris, M. 1987, ApJ, 323, 179
Mamajek, E. E., Barrado y Navascués, D., Randich, S., Jensen, E. L. N., Young, P. A., Miglio, A., & Barnes, S. A. 2008, in ASP Conf. Ser. 384, 14th Cambridge Workshop on Cool Stars, Stellar Systems, and the Sun, ed. G. van Belle (San Francisco, CA: ASP), 374
Mathieu, R. D. 2008, in Handbook of Star Forming Regions, Vol. I: The Northern Sky, ASP Monograph Publications, Vol. 4, ed. B. Reipurth (San Francisco, CA: ASP), 757
Maxted, P. F. L., Jeffries, R. D., Oliveira, J. M., Naylor, T., & Jackson, R. J. 2008, MNRAS, 385, 2210
Mayne, N. J., & Naylor, T. 2008, MNRAS, 386, 261
Metchev, S. A., Eisner, J. A., Hillenbrand, L. A., & Wolf, S. 2005, ApJ, 622, 451
Meyer, M. R., Calvet, N., & Hillenbrand, L. A. 1997, AJ, 114, 288
Millour, F., et al. 2007, A&A, 464, 107
Murdin, P., & Penston, M. V. 1977, MNRAS, 181, 657
Muzerolle, J., D'Alessio, P., Calvet, N., & Hartmann, L. 2004, ApJ, 617, 406
Muzerolle, J., Hillenbrand, L., Calvet, N., Briceño, C., & Hartmann, L. 2003, ApJ, 592, 266
Nesterov, V. V., Kuzmin, A. V., Ashimbaeva, N. T., Volchkov, A. A., Röser, S., & Bastian, U. 1995, A&AS, 110, 367
North, J. R., Tuthill, P. G., Tango, W. J., & Davis, J. 2007, MNRAS, 377, 415
Pedoussaut, A., Carquillat, J. M., Ginestet, N., & Vigneau, J. 1988, A&AS, 75, 441
Pozzo, M., Jeffries, R. D., Naylor, T., Totten, E. J., Harmer, S., & Kenyon, M. 2000, MNRAS, 313, L23
Reach, W., et al. 2006, Infrared Array Camera Data Handbook, Version 3.0 (Pasadena, CA: Spitzer Science Center, Caltech)
Rhee, J. H., Song, I., Zuckerman, B., & McElwain, M. 2007, ApJ, 660, 1556
Rieke, G. H., et al. 2004, ApJS, 154, 25
Rieke, G. H., et al. 2005, ApJ, 620, 1010
Röser, S., Schilbach, E., Schwan, H., Kharchenko, N. V., Piskunov, A. E., & Scholz, R.-D. 2008, A&A, 488, 401
Sacco, G. G., Franciosini, E., Randich, S., & Pallavicini, R. 2008, A&A, 488, 167
Sherry, W. H., Walter, F. M., Wolk, S. J., & Adams, N. R. 2008, AJ, 135, 1616
Sicilia-Aguilar, A., Hartmann, L. W., Hernández, J., Briceño, C., & Calvet, N. 2005, AJ, 130, 188
Sicilia-Aguilar, A., et al. 2006, ApJ, 638, 897

Siegler, N., et al. 2007, ApJ, 654, 580
Siess, L., Dufour, E., & Forestini, M. 2000, A&A, 358, 593
Song, I., Zuckerman, B., Weinberger, A. J., & Becklin, E. E. 2005, Nature, 436, 363
Su, K. Y. L., et al. 2006, ApJ, 653, 675
Sung, H., Stauffer, J. R., & Bessell, M. S. 2009, AJ, 138, 1116
Takeuchi, T., & Artymowicz, P. 2001, ApJ, 557, 990
Uzpen, B., Kobulnicky, H. A., & Kinemuchi, K. 2009, AJ, 137, 3329
van Leeuwen, F. 2007, A&A, 474, 653
Wade, G. A., Bagnulo, S., Drouin, D., Landstreet, J. D., & Monin, D. 2007, MNRAS, 376, 1145
Weidenschilling, S. J. 1997, Icarus, 127, 290
Williams, J. P., & Andrews, S. M. 2006, ApJ, 653, 1480
Wyatt, M. C. 2008, ARA&A, 46, 339
Young, E. T., et al. 2004, ApJS, 154, 428
Zuckerman, B., & Song, I. 2004, ApJ, 603, 738